Overall, the AICEP marks the first use of deep learning in combination with WSI in diagnosis of nasal polyps. It can evaluate the pathologic characterizations of nasal polyps faster and more accurately. We believe that the AICEP will be used widely, in particular in primary hospitals, and even all around the world through the cloud platform.

The authors would like to thank Chunkui Shao (professor, Department of Pathology, The Third Affiliated Hospital of Sun Yat-sen University) and his colleagues for their help.

Qingwu Wu, MD[a]*
Jianning Chen, MD[b]*
Huiyi Deng, MD[a]*
Yong Ren, MSc[c]*
Yueqi Sun, MD, PhD[d]
Weihao Wang, MD[a]
Lianxiong Yuan, MD[e]
Haiyu Hong, MD, PhD[f]
Rui Zheng, MD[a]
Weifeng Kong, MD[a]
Xuekun Huang, MD, PhD[a]
Guifang Huang, BEng[c]
Lunji Wang, BEng[c]
Yana Zhang, MD, PhD[g]
Lanqing Han, MEng[c]
Qintai Yang, MD, PhD[a]

[a]Department of Otorhinolaryngology-Head and Neck Surgery, The Third Affiliated Hospital of Sun Yat-sen University, Guangzhou, China; [b]Department of Pathology, The Third Affiliated Hospital of Sun Yat-sen University, Guangzhou, China; [c]Artificial Intelligence Innovation Center, Research Institute of Tsinghua, Pearl River Delta, Guangzhou, China; [d]Otorhinolaryngology Hospital, The First Affiliated Hospital of Sun Yat-sen University, Guangzhou, China; [e]Department of Science and Research, The Third Affiliated Hospital of Sun Yat-sen University, Guangzhou, China; [f]Department of Otolaryngology-Head and Neck Surgery, The Fifth Affiliated Hospital of Sun Yat-sen University, Zhuhai, China; [g]Feinberg School of Medicine, Northwestern University, Chicago, Ill. E-mail: hanlance@tsinghua-gd.org. Or: yang.qt@163.com.

*The authors contributed equally to this work.

This work was supported by the National Natural Science Foundation of China (grants 81670912 and 81870704), the Industry-Academic Cooperation Foundation of Guangzhou (grant 201704030046), Sun Yat-sen University Clinical Research 5010 Program (grant 2019006), and The Third Affiliated Hospital of Sun Yat-Sen University, Clinical Research Program (grant QHJH201901).

Disclosure of potential conflict of interest: The authors declare that they have no relevant conflicts of interest.

REFERENCES

1. Fokkens WJ, Lund VJ, Mullol J, Bachert C, Alobid I, Baroody F, et al. European position paper on rhinosinusitis and nasal polyps 2012. Rhinol Suppl 2012;23:3, p preceding table of contents, 1-298.
2. Ikeda K, Shiozawa A, Ono N, Kusunoki T, Hirotsu M, Homma H, et al. Subclassification of chronic rhinosinusitis with nasal polyp based on eosinophil and neutrophil. Laryngoscope 2013;123:E1-9.
3. Snidvongs K, Lam M, Sacks R, Earls P, Kalish L, Phillips PS, et al. Structured histopathology profiling of chronic rhinosinusitis in routine practice. Int Forum Allergy Rhinol 2012;2:376-85.
4. Wen W, Liu W, Zhang L, Bai J, Fan Y, Xia W, et al. Increased neutrophilia in nasal polyps reduces the response to oral corticosteroid therapy. J Allergy Clin Immunol 2012;129:1522-8.e1525.
5. Mahdavinia M, Suh LA, Carter RG, Stevens WW, Norton JE, Kato A, et al. Increased noneosinophilic nasal polyps in chronic rhinosinusitis in US second-generation Asians suggest genetic regulation of eosinophilia. J Allergy Clin Immunol 2015;135:576-9.
6. Cao PP, Li HB, Wang BF, Wang SB, You XJ, Cui YH, et al. Distinct immunopathologic characteristics of various types of chronic rhinosinusitis in adult Chinese. J Allergy Clin Immunol 2009;124:478-84, 484.e471-e472.
7. Luo H, Xu G, Li C, He L, Luo L, Wang Z, et al. Real-time artificial intelligence for detection of upper gastrointestinal cancer by endoscopy: a multicentre, case-control, diagnostic study. Lancet Oncol 2019;20:1645-54.
8. Lin H, Li R, Liu Z, Chen J, Yang Y, Chen H, et al. Diagnostic efficacy and therapeutic decision-making capacity of an artificial intelligence platform for childhood cataracts in eye clinics: a multicentre randomized controlled trial. EClinicalMedicine 2019;9:52-9.
9. Long E, Lin H, Liu Z, Wu X, Wang L, Jiang J, et al. An artificial intelligence platform for the multihospital collaborative management of congenital cataracts. Nat Biomed Eng 2017;1.

Available online December 9, 2019.
https://doi.org/10.1016/j.jaci.2019.12.002

Janus kinase inhibition for autoinflammation in patients with *DNASE2* deficiency

To the Editor:

Defective elimination of nucleic acids can trigger autoinflammatory and autoimmune processes.[1] Mice lacking the lysosomal endonuclease DNase II have shown intracellular DNA accumulation, leading to severe anemia and embryonic death.[2] Human subjects carrying homozygous nonsynonymous loss-of-function mutations in *DNASE2* complete gestation but are severely affected by congenital anemia and an inflammatory disorder characterized by splenomegaly, glomerulonephritis, liver fibrosis, circulating anti-DNA autoantibodies, and progressive arthritis.[3]

We describe a patient with a novel hypomorphic homozygous missense mutation in *DNASE2* (c.A284G; p.Y95C) resulting in severe autoinflammation, failure to thrive, hemophagocytic lymphohistiocytosis (HLH), early-onset chronic intestinal inflammation, and suppression of hematopoiesis. Beyond the recent description of this disorder in 3 patients,[3] we further characterize cytokine dysregulation and demonstrate successful treatment with the Janus kinase (JAK) 1/2 inhibitor baricitinib.

The proband (V-2) is a 14-year-old Somalian girl from an endogamous kindred with a history of neonatal anemia (Fig 1, *A*). At 6 years of age, patient V-2 was referred for pyrexia, a history of pancytopenia, hepatosplenomegaly, failure to thrive (height and weight less than the 0.4th percentile), chronic diarrhea, and delayed motor skill development. Investigations (summarized in Table E1 in this article's Online Repository at www.jacionline.org) revealed severe pancytopenia requiring multiple transfusions of red cells and platelets. Intestinal histology from endoscopic biopsy specimens revealed multiple granuloma-like cells within mucosa-associated lymphoid tissue compatible with phagocytosed DNA fragments (pseudogranuloma). Magnetic resonance imaging of the brain revealed biparietal deep white matter parenchymal signal abnormalities (Fig 1, *B*). Bone marrow studies identified macrophage infiltration and associated hemophagocytosis (Fig 1, *C*). At 9 years of age, the patient experienced severe EBV infection, necessitating treatment with dexamethasone and rituximab. Typical HLH criteria were met (see Table E1). She responded partially to the HLH-2004 chemotherapy treatment protocol, which she received for 7 weeks,[4] with cessation of fever and improvement in diarrhea but ongoing pancytopenia and hepatosplenomegaly. For several years, transfusion-dependent anemia, chronic diarrhea, and severe growth retardation were observed.

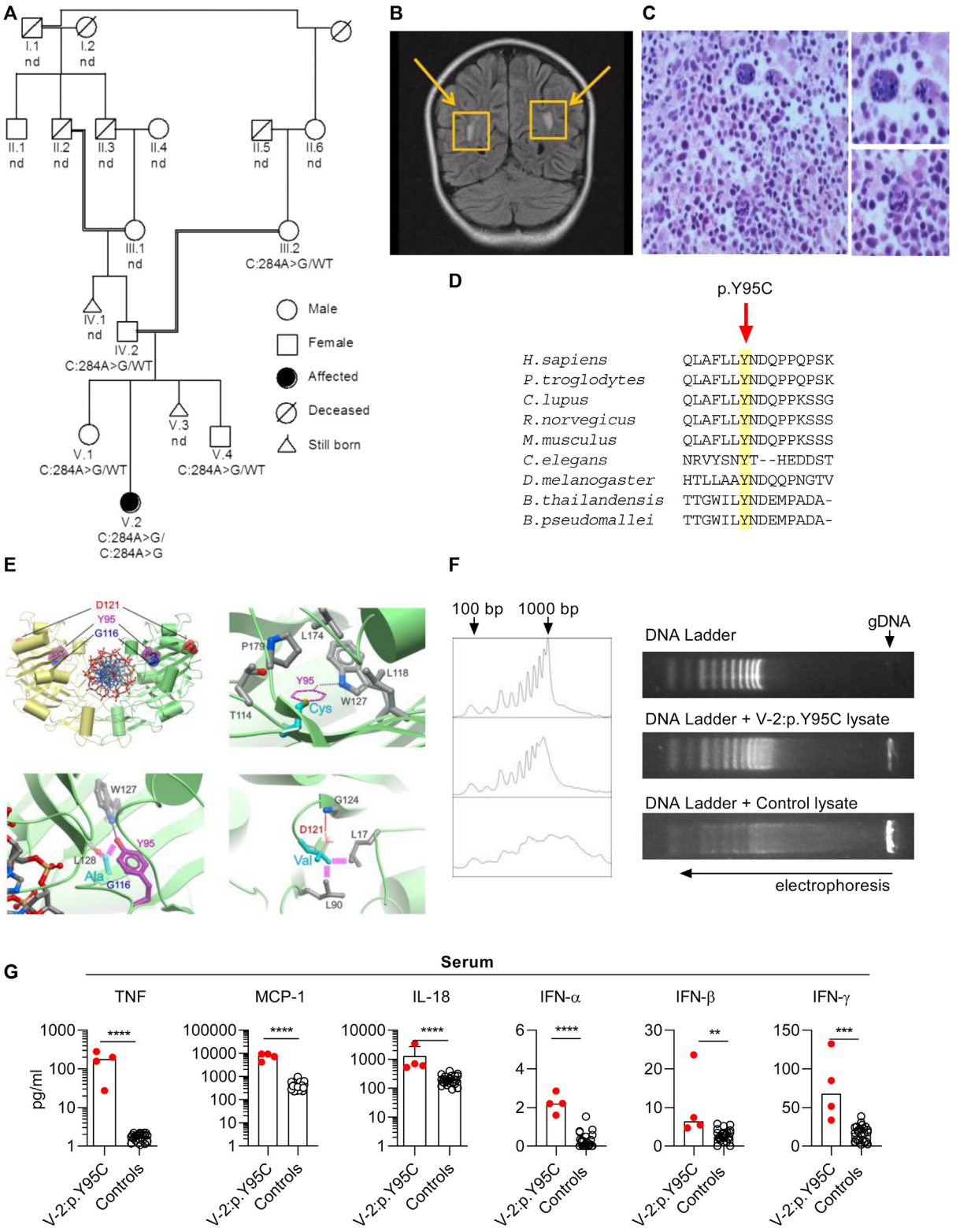

FIG 1. Clinical phenotype of the proband with a homozygous p.Y95C *DNASE2* variant. **A,** Pedigree shows segregation of the p.Y95C homozygous *DNASEII* variant. *nd*, Not determined. **B,** Magnetic resonance image of patient V-2 showing bilateral deep white matter lesions *(yellow arrows)*. **C,** Hemophagocytosis and macrophage infiltration in bone marrow (× 200 magnification on *right*). **D,** Multiple sequence alignment across different species of the p.Y95C mutation. **E,** Predicted crystal structure of DNase II showing the mutations p.Y95C, p.G116A, and p.D121V. **F,** Densitometric quantification of gel band intensity *(left)* and representative agarose gel of lysates from the patient and control subjects incubated with the 1-Kbp ladder *(right)*. *gDNA*, Genomic DNA. **G,** Serum cytokine quantification from patient V-2 (4 time points across 35 months) and healthy donors (n = 24) tested by using Meso Scale Discovery. $^{**}P < .01$, $^{***}P < .001$, and $^{****}P < .0001$, Mann-Whitney *U* test.

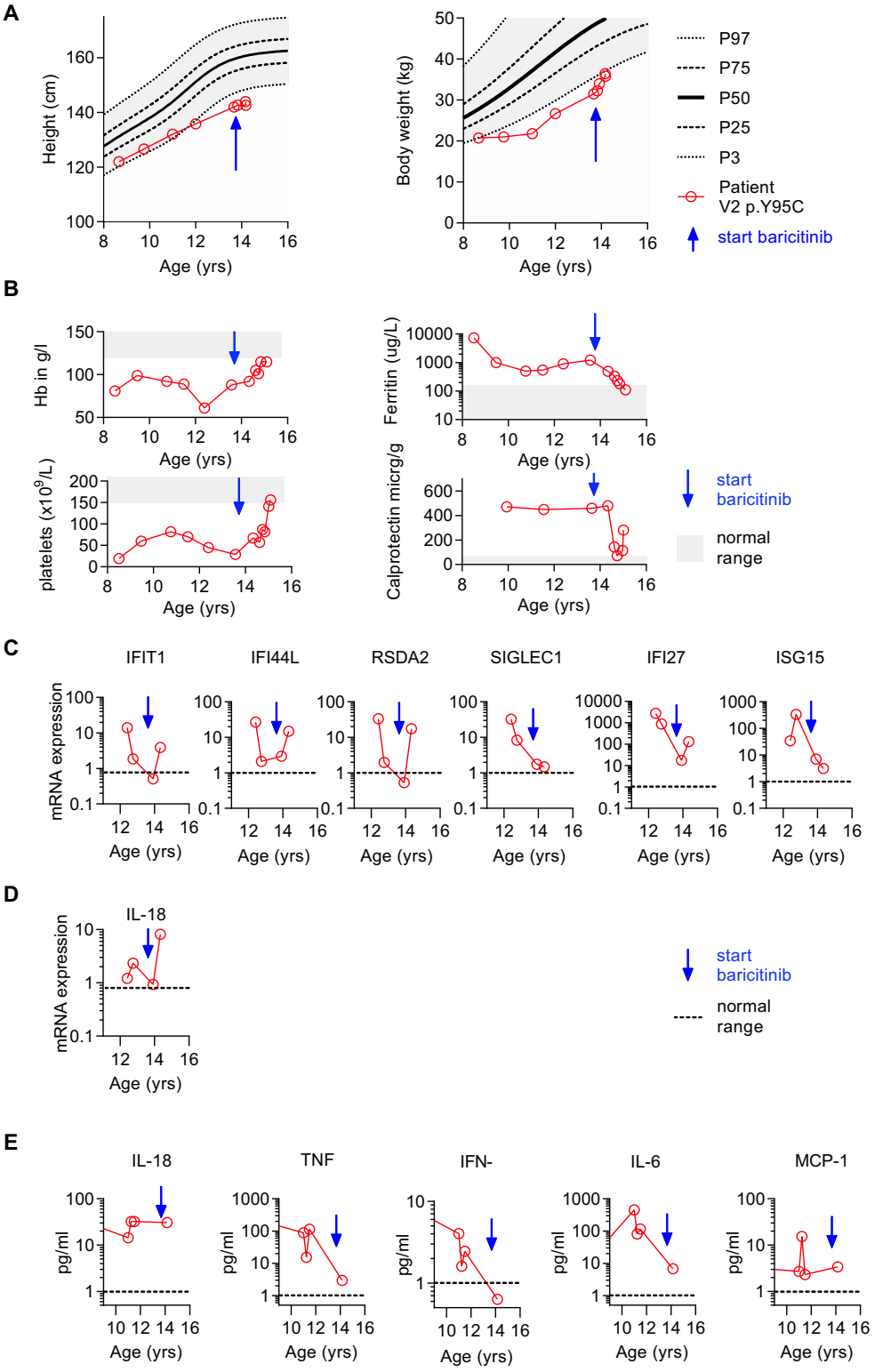

FIG 2. Clinical and immunologic response to JAK1/JAK2 blockade with baricitinib treatment in patient V-2. **A,** Height and weight of patient. *Gray shading*, Normal range; *black lines*, World Health Organization normative data. **B,** Hemoglobin *(Hb)*, ferritin, platelets, and calprotectin levels. *Gray shading* shows the normal range. *Blue arrows* indicate the start of baricitinib. **C** and **D,** Quantitative PCR of a panel of ISGs (Fig 2, *C*) and *IL18* expression (Fig 2, *D*) measured in whole blood of patient V-2 at 2 time points before treatment and 2 time points after treatment normalized to control values. **E,** Serum cytokine Meso Scale Discovery quantification from patient V-2 (collected 2 times before treatment and 1 time after treatment) normalized to control values. *MCP-1*, Monocyte chemoattractant protein 1.

Homozygosity mapping and whole-exome sequencing revealed a rare homozygous variant in *DNASE2* (c.284A>G; p.Y95C; see Fig E1, *A*, and Table E2 in this article's Online Repository at www.jacionline.org). The affected variant is highly conserved across species (Fig 1, *D*). We used structural data of the existing DNase II homodimer complexed with a double-stranded DNA crystal structure from *Burkholderia thailandensis* to model the human DNase II.[5] Residue Y95 is closely packed with residue T114, which is central to the nuclease catalytic HxK motif (H113 and K115), suggesting that small perturbations at residue 95 might have a significant effect on catalytic activity. The 2 recently published mutations in *DNASE2* (p.G116A and p.D121V)[3] will likely disrupt the same catalytic domain (Fig 1, *E*).

The p.Y95C variant completely abolishes DNase II activity in a single radial enzyme diffusion (see Fig E1, *B*) and confers loss of function of the protein rather than absence (see Fig E1, *C* and *D*). Furthermore, granulocyte lysates from patient V-2 confirmed a deficiency in degrading DNA (Fig 1, *F*).

Macrophages show the greatest expression of *DNASE2* and are most likely affected in DNase II–deficient patients (see Fig E2, *A*, in this article's Online Repository at www.jacionline.org). We observed increased lysosomal DNA accumulation in monocyte-derived macrophages from patient V-2 compared with control cells (see Fig E2, *B*). Similarly, clearance of exogenous apoptotic or bacterially derived DNA was reduced in macrophages from patient V-2 (see Fig E2, *C* and *D*).

To investigate whether DNase II deficiency causes a selective DNA degradation defect or broadly affects lysosomal function, we tested antimicrobial activity in macrophages from patient V-2 (see Fig E2, *E*). Normal antimicrobial activity suggests that the defect in patients with *DNASE2* deficiency is restricted to the inability to clear DNA.

Previous studies emphasized that deficiency in *DNASE2* in human subjects and mice results in induction of interferon- and non–interferon-mediated inflammation.[2,3,6,7] Increased levels of TNF, monocyte chemoattractant protein 1, IL-18, IFN-2α, IFN-β, and IFN-γ were detected in sera of patient V-2 (Fig 1, *G*). Increased levels of TNF, IL-1β, interferon-inducible protein 10, and IL-8 were observed in fibroblasts from patient V-2 (see Fig E3, *A*, in this article's Online Repository at www.jacionline.org). p.Y95C macrophages showed high levels of TNF and IL-18, modestly increased levels of IL-1β, and a clear induction of type I interferons (see Fig E3, *B*), which we also confirmed to be present in one of the previously described patients (see Fig E3, *B*).[3]

Type I interferons (IFN-α and IFN-β) bind to type I receptors (IFN-α/β receptor 1/2) and induce the activation of JAK1 and tyrosine kinase 2, leading to signal transducer and activator of transcription 1 and 2 phosphorylation and interferon-stimulated gene (ISG) expression.[8] Because the immunotype of patient V-2 was indicative of a strong ISG signature, we explored JAK inhibition as a therapeutic option. *In vitro* JAK1/JAK2 blockade with baricitinib reduced ISG expression in fibroblasts from control subjects and patient V-2 and control macrophages after IFN-α stimulation (see Fig E4, *A* and *B*, in this article's Online Repository at www.jacionline.org). In contrast, selective blockade of JAK2 using AG490 did not revert the ISG signature (see Fig E4, *A*). In healthy macrophages baricitinib treatment had stronger effects on ISG reduction compared with fibroblasts (see Fig E4, *B*). IFN-α–induced IL-18 levels were reduced after baricitinib or AG490 treatment (see Fig E4, *C*), suggesting a contribution of JAK2 signaling to IL-18 production in control macrophages.

Because JAK inhibitors are effective in several interferonopathies[9] and baricitinib reverted the inflammatory signature in fibroblasts and macrophages *in vitro*, we treated our otherwise therapy-nonresponsive patient with baricitinib. We started with a 2-mg oral dose once daily, increasing weekly by 2 mg to achieve a final target dose of 6 mg (2 mg 3 times a day). Baricitinib was well tolerated with no adverse events and resulted in rapid and sustained clinical improvement (now for >6 months). In particular, the improved energy levels reported by the patient and the ability to attend school full-time were relevant patient-reported outcomes. Weight gain improved (Fig 2, *A*), and the patient underwent menarche 4 months after starting baricitinib. Blood parameters (Fig 2, *B*), gastrointestinal symptoms, and fecal calprotectin levels improved (Fig 2, *B*). Baricitinib decreased ISG expression in peripheral blood and cytokine levels compared with pretreatment levels (Fig 2, *C-E*). After 6 months of treatment, however, although the ISG signature indicated normalization of *SIGLEC1* and *ISG15*, there was an upward trend of *IFIT1*, *IFI44L*, *RSDA2*, *IL18*, and *IFI27*, despite ongoing therapeutic response. Our data suggest that JAK1/2 inhibition is a rational and effective treatment for DNase II deficiency.

In conclusion, we describe an additional patient with human DNase II deficiency who presented with HLH and early-onset intestinal inflammation, expanding the phenotypic spectrum of DNase II deficiency. We characterize the mechanisms underpinning the complex immunophenotype and show in a single patient that blocking JAK1/JAK2 with baricitinib can be used to curb pathologic interferon signaling caused by an inability to clear intracellular DNA.

We thank the patients and their families, as well as healthy volunteers, for consenting to this research. We thank Yanick Crow, Jan Rehwinkel, Anne Bridgeman, Jonny Hertzog, and Julie Schulthess for critical input and research materials.

Ying Hong, PhD[a]*
Melania Capitani, PhD[b]*
Claire Murphy, PhD[a,c]
Sumeet Pandey, PhD[b]
Athena Cavounidis, MSc[b]
Haruo Takeshita, PhD[d]
Sira Nanthapisal, PhD[a,e]
Toshihiro Yasuda, PhD[f]
Brigitte Bader-Meunier, MD[g]
Dara McCreary, MSc[a]
Ebun Omoyinmi, PhD[a]
Anupama Rao, MD[c]
Claire Booth, PhD[a,c]
Kimberly Gilmour, PhD[c]
Neil Sebire, PhD[c]
Neil Shah, PhD[c]
Nigel Klein, PhD[a,c]
Alex N. Bullock, PhD[h]
Despina Eleftheriou, PhD[a,c,i]
Holm H. Uhlig, MD, DPhil[b]‡
Paul Brogan, PhD[a,c]‡

From [a]University College London Great Ormond Street Institute of Child Health, London, United Kingdom; [b]the Translational Gastroenterology Unit, Department of Pediatrics, and Oxford Biomedical Research Centre (BRC), University of Oxford, Oxford, United Kingdom; [c]Great Ormond Street Hospital for Children NHS Foundation Trust, London, United Kingdom; [d]the Department of Legal Medicine, Shimane University, Shimane, Japan; [e]Thammasat University, Bangkok, Thailand; [f]the Department of

Medical Genetics and Biochemistry, University of Fukui, Fukui, Japan; [g]the Department of Pediatric Immunology and Rheumatology, Hôpital Necker-Enfants Malades, Assistance Publique-Hôpitaux de Paris, Paris, France; [h]the Structural Genomics Consortium, Nuffield Department of Medicine, University of Oxford, Oxford, United Kingdom; and [i]the Arthritis Research UK Centre for Adolescent Rheumatology, UCL, London, United Kingdom. E-mail: y.hong@ucl.ac.uk.

*These authors contributed equally to this work

‡These authors contributed equally to this work.

This work was funded in part by Rosetrees, Great Ormond Street Hospital Children's Charity, and Versus Arthritis (grants 21791, 21593 and 21064). All research at the Great Ormond Street Hospital National Health Service (NHS) Foundation Trust and UCL Great Ormond Street Institute of Child Health is made possible by the National Institute of Health Research (NIHR)'s Great Ormond Street Hospital Biomedical Research Centre (BRC). The views expressed are those of the authors and not necessarily those of the NHS, the NIHR, or the Department of Health. We acknowledge support for set-up of pilot experiments by the BRC to the Oxford GI biobank (11/YH/0020 and 16/YH/0247). The research was also supported by the NIHR Oxford Biomedical Research Centre (BRC), University of Oxford, Wellcome Trust (grant 106169/ZZ14/Z), and the Structural Genomics Consortium SGC. H.H.U. is supported by NIHR Oxford BRC and the Leona M. and Harry B. Helmsley Charitable Trust.

Disclosure of potential conflict of interest: C. Booth received consultancy fees from Novimmune and SOBI. D. Eleftheriou received institutional grants from Lilly, Roche, and Pfizer. H. H. Uhlig received research support or consultancy fees from UCB Pharma, Eli Lilly, Boehringer Ingelheim, Pfizer, Celgene, and AbbVie. P. Brogan has received institutional grants from Novartis, SOBI, Roche, Chemocentryx, and Novimmune; consultancy fees from Roche, Novartis, and SOBI; and speaker's fees from UCB.

REFERENCES

1. Lazear HM, Schoggins JW, Diamond MS. Shared and distinct functions of type I and type III interferons. Immunity 2019;50:907-23.
2. Kawane K. Requirement of DNase II for definitive erythropoiesis in the mouse fetal liver. Science 2001;292:1546-9.
3. Rodero MP, Tesser A, Bartok E, Rice GI, Della Mina E, Depp M, et al. Type I interferon-mediated autoinflammation due to DNase II deficiency. Nat Commun 2017;8:2176.
4. Henter J-I, Horne A, Aricó M, Egeler RM, Filipovich AH, Imashuku S, et al. HLH-2004: diagnostic and therapeutic guidelines for hemophagocytic lymphohistiocytosis. Pediatr Blood Cancer 2007;48:124-31.
5. Varela-Ramirez A, Abendroth J, Mejia AA, Phan IQ, Lorimer DD, Edwards TE, et al. Structure of acid deoxyribonuclease. Nucleic Acids Res 2017;45:6217-27.
6. Pawaria S, Moody K, Busto P, Nündel K, Choi C-H, Ghayur T, et al. Cutting edge: DNase II deficiency prevents activation of autoreactive B cells by double-stranded DNA endogenous ligands. J Immunol 2015;194:1403-7.
7. Kawane K, Tanaka H, Kitahara Y, Shimaoka S, Nagata S. Cytokine-dependent but acquired immunity-independent arthritis caused by DNA escaped from degradation. Proc Natl Acad Sci U S A 2010;107:19432-7.
8. Ivashkiv LB, Donlin LT. Regulation of type I interferon responses. Nat Rev Immunol 2014;14:36-49.
9. Sanchez GAM, Reinhardt A, Ramsey S, Wittkowski H, Hashkes PJ, Berkun Y, et al. JAK1/2 inhibition with baricitinib in the treatment of autoinflammatory interferonopathies. J Clin Invest 2018;128:3041-52.

Available online November 24, 2019.
https://doi.org/10.1016/j.jaci.2019.11.020

Three-year follow-up after peanut food challenges: Accidental reactions in allergic children and introduction failure in tolerant children

To the Editor:

The gold standard to diagnose peanut allergy is a double-blind, placebo-controlled food challenge (DBPCFC).[1] Children and parents are advised to avoid peanut after a positive DBPCFC result or to introduce peanut after a negative DBPCFC result. Children with confirmed peanut allergy have frequent accidental allergic reactions and often do not recognize and adequately treat allergic symptoms.[2] On the other hand, children with a negative DBPCFC result often experience failure to introduce peanut at home.[3] Children and parents might benefit from a DBPCFC because our previous systematic review reported that health-related quality of life (HRQL) improved up to 6 months after an oral food challenge, irrespective of the outcome.[4] Limited data exist on the long-term follow-up after a DBPCFC, including the frequency and treatment of accidental allergic reactions, diet, and HRQL.

We sought to evaluate 1) allergic reactions and HRQL in children with peanut allergy and 2) peanut introduction and HRQL in peanut-tolerant children. The current study is a 3-year follow-up of 83 children who participated in a prospective study in The Netherlands and all underwent a DBPCFC for peanut.[5] Three years after the DBPCFC, all parents and children aged 8 years or older were contacted by mail and asked to fill out a questionnaire on accidental allergic reactions and current diet and the Food Allergy Quality of Life Questionnaire (FAQLQ). Details on data collection and statistical methods are presented in the Methods section in this article's Online Repository at www.jacionline.org. The study was approved by the ethics committee of the University Medical Centre Utrecht, and written informed consent was obtained before enrollment in the original study.

In total, 69 (83%) of 83 children completed the questionnaire after a positive (n = 41/48) or negative (n = 28/35) DBPCFC result. Children who completed the questionnaire and children who did not were comparable in age, sex, sensitization, and HRQL and DBPCFC outcomes (data not shown). The mean (SD) age of the children at follow-up was 11.5 (SD, 3.5) years, and 48 (70%) were male. The study flowchart and baseline characteristics are presented in Fig E1 and Table E1 in this article's Online Repository at www.jacionline.org.

Seventeen (41%) of 41 children with peanut allergy had a total of 68 accidental allergic reactions to peanut during the 3-year follow-up. Children with peanut allergy and accidental allergic reactions were comparable with those without accidental allergic reactions (see Table E2 in this article's Online Repository at www.jacionline.org). The characteristics of the most severe reactions are presented in Table I (see also Table E3 in this article's Online Repository at www.jacionline.org).[6] All children had symptoms within 2 hours from ingestion. Five of 17 children had mild or moderate symptoms and used antihistamines at home. Twelve of 17 children reported severe symptoms and used antihistamines (n = 7), antihistamines and oral steroids (n = 1), bronchodilators (n = 1), or no medication at all (n = 3). Seven of 17 children reported severe lower respiratory tract symptoms. None of these 7 children used their epinephrine autoinjectors.

Parent-proxy–reported HRQL remained unchanged between baseline and 3-year follow-up in children with peanut allergy (mean difference [MD], 0.05; $P = .823$). On the individual level, HRQL improved in 29% and deteriorated in 39% of children with peanut allergy 3 years after the DBPCFC compared with baseline values. HRQL data are presented in Fig E2 and Table E4 in this article's Online Repository at www.jacionline.org.

Long-term introduction of peanut 3 years after the DBPCFC failed in 9 (32%) of 28 peanut-tolerant children (Fig 1). The reported reasons for failure were aversion (n = 5), aversion and fear (n = 2), or fear (n = 2). Parent-proxy–reported HRQL improved significantly and was clinically relevant during

METHODS

Study participants

This study was approved by the Bloomsbury Ethics Committee (no. 08H071382), the Oxford GI biobank (no. 09/H1204/30), and the Comité de Protection des Personnes (ID-RCB/EUDRACT 2014-A01017-40) in France. We obtained written informed consent from all family members and adolescent healthy control subjects with local ethics approval (REC 11/LO/0330).

Genetic mapping and sequencing

All 5 family members were genotyped with the Illumina cytoSNP12 chip (Illumina, San Diego, Calif). Two hundred nanograms of DNA was isothermally amplified overnight and then enzymatically fragmented. The fragmented DNA was incubated on a BeadChip overnight. These were imaged with the Illumina iScan System. Regions of homozygosity were identified by using the Illumina BeadStudio with the loss-of-heterozygosity detector plug-in (version 1.0.3). The minimum number of contiguous homozygous single nucleotide polymorphisms was set to 100.

Whole-exome sequencing was completed by using the Illumina platform and sequenced on the Illumina HiSeq2000. Raw sequence data were aligned to the human reference genome by using the Burrows-Wheeler Aligner algorithm. Variant calling was performed with the Genome Analysis Toolkit, and variants were annotated with wANNOVAR.

The *DNASE2* variant was confirmed and familial segregation was ascertained by using PCR and Sanger sequencing with the following primers to amplify and sequence exon 3: forward, GCCTTCTCTTCCCTCTCTCC; reverse, GTCAGGGGTTACCTTGGAAAAAT. Sanger sequencing was performed with the AB3730 Analyzer with the BigDye v3.1 kit (Applied Biosystems, Foster City, Calif).

Protein sequence alignment

Multiple *DNASE2* sequences were aligned by using ClustalW2.[E1] Data obtained from the sequence alignment are based on the following National Center for Biotechnology Information accession numbers: *Homo sapiens*, AAH10419.3; *Rattus norvegicus*, NP_612548.1; *Pan troglodytes*, XP_001170388.1; *Canis lupus*, XP_533902.3; *Mus musculus*, NP_034192.1; *Drosophila melanogaster*, NP_650672.1; *Caenorhabditis elegans*, NP_491414; *Burkholderia thailandensis*, WP_009895252.1; and *Burkholderia pseudomallei*, YP_111989.1.

Structural modeling

Structural models and figures were prepared by using the ICM software package (MolSoft, San Diego, Calif). A homology model for human DNase II was prepared by using the existing structure from *B thailandensis* (PDB 5UNB) as the model template. Double-stranded DNA (PDB 2BNA) was positioned manually at the dimer interface to indicate the potential DNA-binding surface, as previously highlighted.[E2] All coordinate files were obtained from the Protein Data Bank (http://www.rcsb.org).

PBMC isolation and monocyte-derived macrophage cell culture

PBMCs were isolated from 15 mL of blood from the patient and control subjects by using density gradient centrifugation (Lymphoprep; STEMCELL Technologies, Vancouver, British Columbia, Canada) and cultured in RPMI 1640 with glutamine (Sigma-Aldrich, St Louis, Mo) supplemented with 10% FCS. PBMCs (4×10^6) were plated, and after 2 hours, adherent monocytes were washed and cultured in the presence of 100 ng/mL macrophage colony-stimulating factor (PeproTech, Rocky Hill, NJ) for 5 days to differentiate them to macrophages. PBMCs were sorted with fluorescence-activated cell sorting from healthy donor blood by using canonical cell population surface markers: dendritic cell $CD1c^+$ (clone B-Ly6; BD Biosciences, Franklin Lake, NJ), B-cell $CD19^+$ (clone HIB19; BioLegend, San Diego, Calif) and $CD8^+$ (clone RPA-T8; BD Biosciences), T-cell $CD4^+$ (clone RM4-5; BioLegend), T memory cell CD45RO (clone UCHL1, BioLegend) and CCR7 (clone G043H7, BioLegend), T-cell $CD8^+$ (clone RPA-T8; BD Biosciences), DR+11C- (clone B-Ly6; BD Biosciences), natural killer cell $CD16^+$ (clone 3G8; BioLegend), myeloid dendritic cell $CD141^+$ (clone M80; BioLegend), and monocyte $CD14^+$ (clone M5E2; BioLegend).

DNA degradation assay in granulocytes and COS-7 cells

Granulocytes were purified from the precipitate after the blood gradient by removing red blood cells with ACK Lysing Buffer (Invitrogen, Carlsbad, Calif). Granulocytes (3.5×10^6) from the patient and control subjects were lysed in 40 μL of lysis buffer (25 mmol/L Tris-HCl [pH 7.6], 150 mmol/L NaCl, 5 mmol/L ethylenediamine tetra-acetic acid, 1% NP-40 or 1% Triton X-100, 1% sodium deoxycholate, and 0.1% SDS) at pH 5.5 in the presence of proteinase and phosphate inhibitors. Lysates were spun down at 14,000 rpm for 15 minutes, and supernatants were collected. Each lysate was split in 2: 20 μL incubated with 2 μL of 1-Kbp DNA ladder solution (Bioline, London, United Kingdom) and 20 μL without. Samples were incubated for 90 minutes at 37oC. Ten microliters of each sample was loaded on agarose gel (1.5%) and run under an electric field at 110 V in the presence of TAE 1 × buffer for 1 hour. Gel pictures were acquired on the UVP BioImaging System (Analytik Jena US LLC). Gel densitometric analysis was done with ImageJ software (National Institutes of Health, Bethesda, Md).

The human *DNASE2* cDNA sequence was cloned into the expression vector pcDNA3.1 (+; Invitrogen)[E3] and used as a wild-type construct. The variant construct corresponding to p.Y95C in *DNASE2* was inserted into the wild-type template by using the KOD-Plus Mutagenesis kit (Toyobo, Osaka, Japan). Nucleotide sequences of the construct were confirmed by using DNA sequence analysis. Purification of each construct used for transfection was performed with the Plasmid Midi Kit (Qiagen, Hilden, Germany).

DNase II activity in the transfected COS-7 cells was assayed by using the single radial enzyme diffusion method with an LAS-3000 imaging analyzer (Fuji Film, Tokyo, Japan), according to our previous reports.[E4] The activity of wild-type DNase II was defined as 1.0, and that of the amino acid–substituted DNase II was expressed relative to the wild-type.

Immunofluorescence cell staining

Macrophages (2×10^5) from control subjects and the patient were seeded on a Cyto Chamber and left to adhere for 2 hours. Subsequently, they were stained with 4′-6-diamidino-2-phenylindole dihydrochloride (1 μg/mL; Sigma-Aldrich) for 20 minutes and washed twice with PBS.

To evaluate the ability of macrophages to process DNA from engulfed apoptotic cells, they were cocultured for 4 hours with SYBR Green (1:10,000; Life Technologies, Grand Island, NY)–positive HEK 293 apoptotic cells at a 1:1 ratio. Apoptosis was induced by means of exposure under a UV lamp for 20 minutes after 4 hours of culture; the apoptotic status was confirmed by using fluorescence-activated cell sorting staining for Annexin V and 7-aminoactinomycin D. Moreover, to evaluate the ability of macrophages to process DNA from invasive *Salmonella* species, they were infected for 1 hour with SYTO 9 (50 nmol/L; Life Technologies)–positive bacteria at a multiplicity of infection of 1:10 and then left for 4 hours under gentamicin treatment. In all conditions, 2 hours before the end of incubation, macrophages were stained with LysoTracker Deep Red (Thermo Fisher, Waltham, Mass) 1:2000 solution. Cells were fixed with PBS–paraformaldehyde 4% solution for 10 minutes at 37°C and then washed. Slides were mounted with a glass coverslip by using VECTASHIELD solution (Vector Laboratories, Burlingame, Calif). Images were captured with a Nikon eclipse ME600 fluorescence microscope (Nikon, Tokyo, Japan) and analyzed with ImageJ software.

Gentamicin protection assay

Macrophages at day 5 of differentiation were detached with Versene solution (Gibco, Carlsbad, Calif) for 5 minutes and counted. Macrophages (2×10^4) were seeded per well in 96-well plates. Then they were infected with

Salmonella typhimurium at a multiplicity of infection of 1:10 for 1 hour, followed by 2 hours of treatment with 100 μg/mL gentamicin (Sigma-Aldrich). Cells were then placed in lysates with 50 μL of Triton 1 × . Undiluted and diluted 1:10 and 1:100 cell lysates were plated in LB-agar plates that were incubated overnight at 37°C. Bacterial colonies were counted manually.

Macrophage and fibroblast stimulations

Healthy donor macrophages (1×10^5 cells) and fibroblasts (1×10^5 cells) were either left untreated or treated with baricitinib (300 nmol/L; Cayman Chemical, Ann Arbor, Mich), AG490 (20 μmol/L; Calbiochem, Nottingham, United Kingdom), and filgotinib (200 nmol/L; Cayman Chemicals) for 1 hour in a 48-well plate. After treatment, both macrophages and fibroblasts were either left unstimulated or stimulated with IFN-α (10 U/mL; R&D Systems, Minneapolis, Minn) for 24 hours in the presence of the drug.

RNA expression analysis in total blood, fibroblasts, and macrophages

Whole blood was collected into PAXgene tubes (BD Biosciences). We used a PreAnalytix RNA isolation kit for whole blood and the RNeasy Micro Kit (Qiagen) for RNA isolation from macrophages and fibroblasts. The RNA concentration was assessed with a Nanodrop (FLUOstar Omega; Labtech, Orternberg, Germany). Total RNA was retrotranscribed to cDNA by using the Reverse Transcription kit (Applied Biosystems). We performed quantitative PCR analysis using the iTaq Universal SYBR Green Supermix (172-5121; Bio-Rad Laboratories, Hercules, Calif) and the TaqMan Gene Expression Assay (FAM; Applied Biosystems).

The relative abundance of each of 6 "interferon score" targets (*IFL27*, *IFIT1*, *IFI44L*, *ISG15*, and *RSAD2*) and other proinflammatory transcripts was normalized to the expression level of *HPRT1* or *RPLPO* assessed by using Bio-Rad CFX Maestro software.

Cytokine protein analysis using ELISA and multiplex assay

Cytokine levels were measured in the sera of patients and control subjects and in supernatants of fibroblasts using a Meso Scale Discovery multiplex kit (Meso Scale Diagnostics, Rockville, Md), according to the manufacturer's instructions. Control sera was obtained from adolescent healthy control subjects with local ethics approval (REC reference 11/LO/0330; $n = 24$; 13 male subjects; median age, 15.7 years; range, 10.7-17.5 years). Undiluted macrophage supernatants were assayed for TNF, IL-1β, and IL-18 cytokines using the ProcartaPlex-Multiplex Immunoassay (Invitrogen).

Statistical analyses

All statistical (ANOVA or the Mann-Whitney *U* test) graphs were produced with Prism software (version 8; GraphPad Software). All experiments were repeated at a minimum in triplicates, unless otherwise specified. *P* values of less than .05 were considered significant.

E-REFERENCES

E1. Goujon M, McWilliam H, Li W, Valentin F, Squizzato S, Paern J, et al. A new bioinformatics analysis tools framework at EMBL-EBI. Nucleic Acids Res 2010; 38(Web Server):W695-9.

E2. Varela-Ramirez A, Abendroth J, Mejia AA, Phan IQ, Lorimer DD, Edwards TE, et al. Structure of acid deoxyribonuclease. Nucleic Acids Res 2017;45:6217-27.

E3. Takeshita H, Yasuda T, Iida R, Nakajima T, Hosomi O, Nakashima Y, et al. Identification of the three non-identical subunits constituting human deoxyribonuclease II. FEBS Lett 1998;440:239-42.

E4. Ueki M, Takeshita H, Fujihara J, Kimura-Kataoka K, Iida R, Yuasa I, et al. Genetic and expression analysis of all 7 non-synonymous single nucleotide polymorphisms in the human deoxyribonuclease II gene, with potential relevance to autoimmunity. Clin Chim Acta 2010;411:92-8.

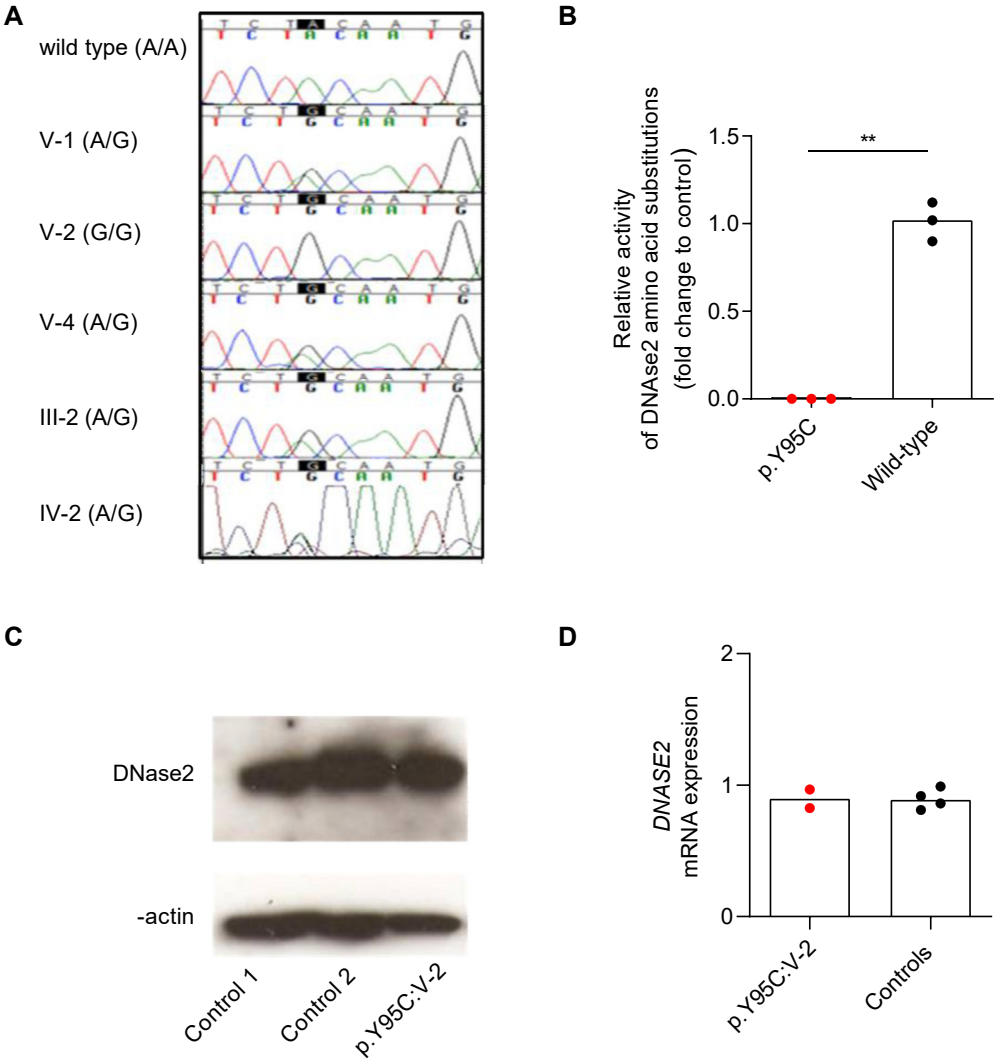

FIG E1. Homozygous mutation that leads to loss of function of *DNASE2* but not to mRNA or protein level changes in cells. **A,** Sanger sequencing chromatogram of *DNASE2* aligned to reference exon 3 (NM_001375) at position c.284 showing a heterozygous pattern with parents (IV-2 and III-2) and unaffected siblings (V-1 and V-4) of the proband and homozygosity for G in the affected proband (V-2). **B,** A single radial enzyme diffusion assay revealed that substitution of the tyrosine at amino acid 95 with a cysteine (p.Y95C) completely abolishes DNase II activity in COS-7 cells. $^{**}P < .01$. **C** and **D,** There was no change in *DNASE2* protein (Fig 1, *C*) or mRNA (Fig 1, *D*) expression in dermal fibroblasts from patient V-2.

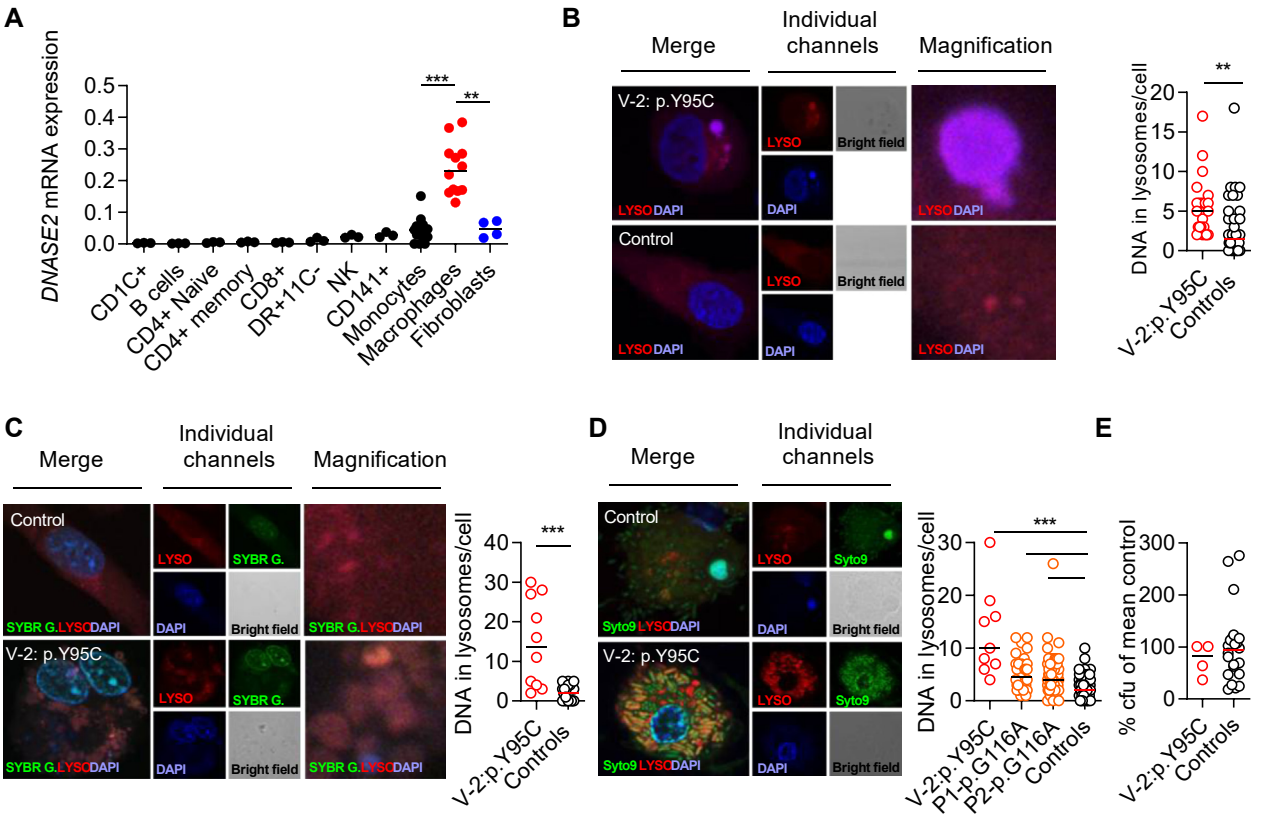

FIG E2. Macrophages with the homozygous *DNASE2* p.Y95C variant have impaired DNA clearance ability. **A,** *DNASE2* gene expression of sorted human cells from healthy control subjects reveals that macrophages show the greatest expression of *DNASE2*. $^{**}P < .01$ and $^{***}P < .0001$. **B,** Confocal image *(left)* and quantification of DNA in lysosomes *(right)* of macrophages from the patient and control subjects stained with 4′-6-diamidino-2-phenylindole dihydrochloride (DAPI) and LysoTracker. There was increased lysosomal DNA accumulation in monocyte-derived macrophages from patient V-2 compared with control subjects. $^{**}P < .01$. **C** and **F,** Confocal image *(left)* and quantification of exogenous DNA in lysosomes per cell *(right)* of macrophages from patients and control subjects stained with DAPI and then cocultured with SYBR Green–positive apoptotic HEK 293 cells (Fig 2, *C*) and prestained SYTO 9–*Salmonella* (multiplicity of infection = 20; Fig 2, *D*). Monocyte-derived macrophages from patient V-2 and 2 previously reported siblings with the homozygous p.G116A mutation showed reduced clearance of exogenous apoptotic or bacterially derived DNA. $^{***}P < .001$. **E,** Gentamicin protection assay of monocyte-derived macrophages from patient V-2 and control subjects showed normal antimicrobial activity. The graph represents pooled data of colony-forming unit quantification.

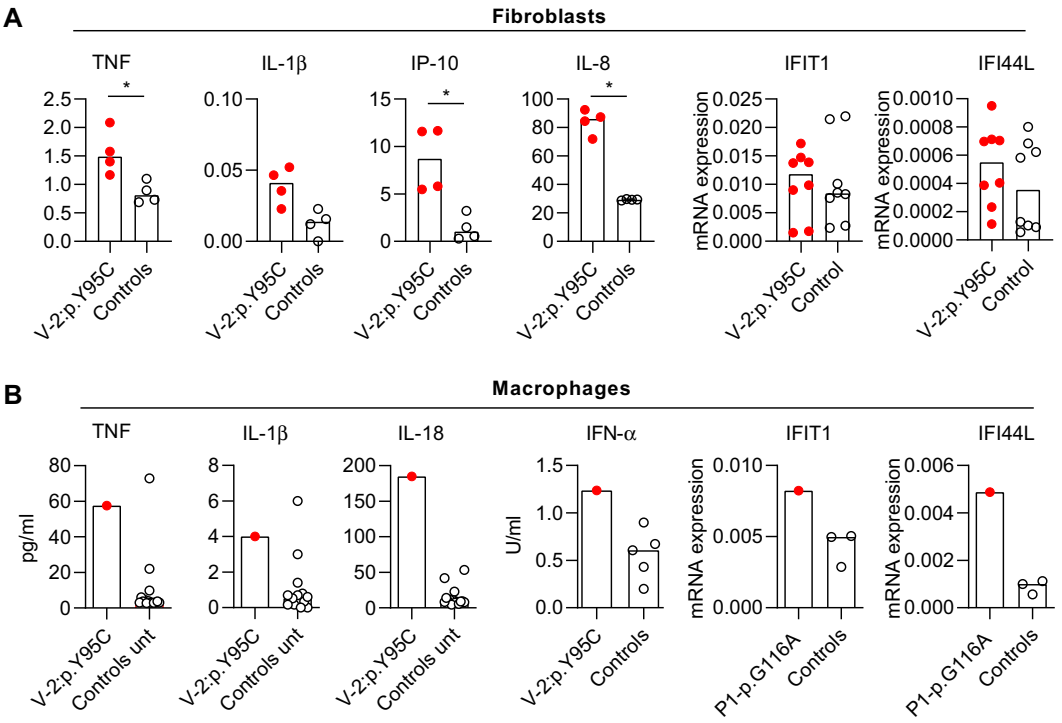

FIG E3. Proinflammatory cytokine profile in fibroblasts and macrophages derived from proband V-2 with the homozygous p.Y95C *DNASE2* variant. **A,** Increased levels of cytokines (TNF, IL-1β, interferon-inducible protein 10 *[IP-10]*, and IL-8) quantified by means of ELISA and upregulation of gene expression of the ISGs (*IFIT1* and *IFI44L*) in fibroblasts from patient V-2 compared with control cells. **B,** Increased levels of cytokines (TNF, IL-18, and IL-1β) quantified by using Luminex and upregulation of gene expression of the ISGs (*IFIT1* and *IFI44L*) in macrophages from patient V-2 compared with control cells. Gene expression of ISGs (*IFIT1* and *IFI44L*) in macrophages from a patient with the homozygous *DNASE2* p.G116A variant and healthy control macrophages was also performed and is presented for comparison.

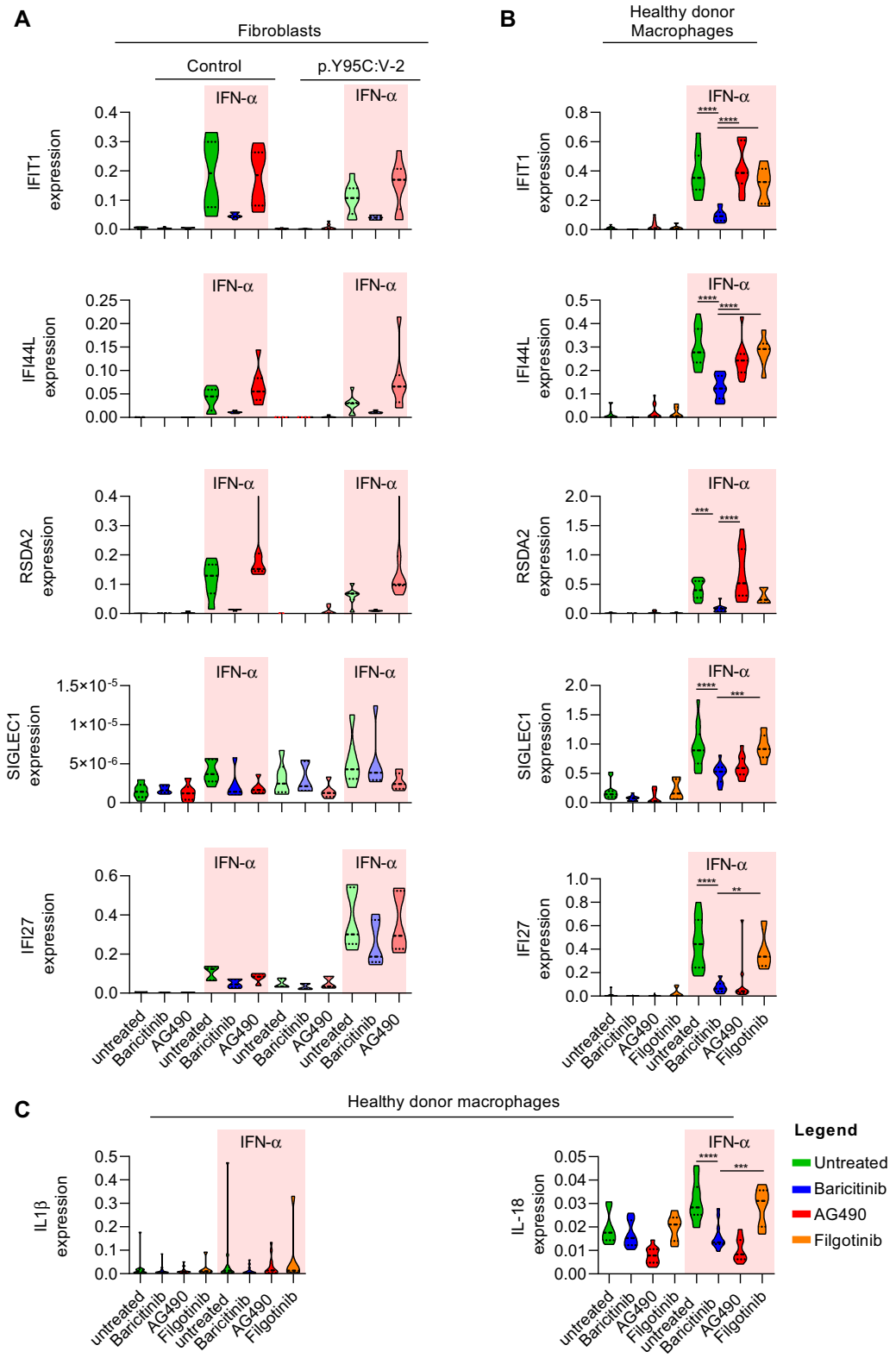

FIG E4. Effect of *in vitro* JAK1/JAK2 blockade on type I interferon signature and IL-18 expression. **A,** Quantitative RT-PCR of ISGs (*IFIT1*, *IFI44L*, *RSDA2*, *SIGLEC1*, and *IFI27*) from patient V-2 and control fibroblasts with and without IFN-α stimulation in the presence and absence of baricitinib (JAK1/JAK2 blockade), AG490 (selective JAK2 blockade), and filgotinib (selective JAK1 blockade) for 24 hours. **B,** Quantitative PCR of ISGs (*IFIT1*, *IFI44L*, *RSDA2*, *SIGLEC1*, and *IFI27*) from healthy donor macrophages stimulated with and without IFN-α in the presence and absence of baricitinib or AG490 for 24 hours. **C,** Quantitative PCR of *IL18* and *IL1B* genes from healthy donor macrophages stimulated with and without IFN-α in the presence and absence of baricitinib and AG490 for 24 hours. $^{**}P < .01$, $^{***}P < .001$, and $^{****}P < .0001$.

TABLE E1. Patient V-2's laboratory investigations

Laboratory investigations	Patient V-2 (reference range)
Autoantibodies persistent >3 mo	Absent†
Hemoglobin*	50 g/L‡ (120-160 g/L)
Platelet count*	21 × 10^9/L§ (150-450 × 10^9/L)
White blood cell count*	0.24 × 10^9/L‖ (4.0-11 × 10^9/L)
Triglycerides*	3.98 mmol/L (0.32-1.46 mmol/L)
Fibrinogen	2.9 g/L (1.7-4.0 g/L)
Monocyte and lymphocyte subsets	Lymphopenia¶ Normal αβ double-negative T cells Normal γδ T cells
Naive T-cell subsets	Variable#
IgG	19.9 g/L (3.1-13.8 g/L)
IgA	1.94 g/L (0.4-0.7 g/L)
IgM	2.29 g/L (0.5-2.2 g/L)
IgD	7 kU/L (2-100 kU/L)
IgE	5.1 kU/L (0-48 kU/L)
MHC class I expression	Normal
T-cell Vβ repertoire	Consistent with polyclonal T cells
IL-2–inducible T-cell kinase ITK immunoblot	Normal
Nitroblue tetrazolium test	Normal
Vaccine responses	Variable**
Perforin expression (CD56 cells)	Normal††
Perforin gene sequencing	No damaging mutations‡‡
CD107a granule release (CD8 and NK cells)	CD8 CD107a$^+$: control, 5.0%; patient, 6.9% NK CD107a: control, 13.7%; patient, 23.1%
Natural killer cytotoxicity test*	Abnormal§§
Gene sequencing for known causes of HLH and immunodeficiency‖‖‖	No known disease-causing mutations identified
T-cell receptor excision circles	1902 (>10,000/million T cells)¶¶
Soluble CD25*	7624 pg/mL## (<2500 pg/mL)***
Complement C3	1.49 g/L (0.75-1.65 g/L)
Complement C4	0.45 g/L (0.14-0.54 g/L)
Fecal calprotectin	472 mg/kg††† (<50 mg/kg)
Ferritin*	7371 μg/L‡‡‡ (12-81 μg/L)
Liver enzymes	Alanine aminotransferase, 219 U/L (10-25 U/L) Alkaline phosphatase, 96 U/L (150-380 U/L)
PHA stimulation	Variable§§§

NK, Natural killer.

*Laboratory features contributing to the diagnosis of HLH. Other clinical features supporting the diagnosis of HLH included fever, hepatosplenomegaly, and hemophagocytosis demonstrated in bone marrow aspirate (see main text).

†Autoantibodies tested: anti-nuclear antibodies, anti-neutrophil cytoplasm antibodies, rheumatoid factor, anti-tissue transglutaminase antibodies, and anti-thyroid peroxidase antibodies.

‡Lowest hemoglobin level of 147 measurements.

§Lowest platelet count of 147 measurements.

‖Lowest white blood cell count of 147 measurements.

¶Normal proportions of T, B, and natural killer cells but in low numbers.

#Test repeated 4 times; normal proportion of naive cells on 3 occasions (54% to 64%) and numbers of reduced naive T cells for age on 1 occasion (35%).

**IgG antibodies to tetanus normal (0.04 IU/mL; range, >0.1 IU/mL); IgG antibodies to pneumococcus (all <0.35 μg/mL; range, >0.35 μg/mL).

††Very few cells available for analysis. Perforin was expressed, but quantification was not possible.

‡‡One synonymous polymorphism in *PRF1*, c.C900T p.H330H, identified with an Exome Aggregation Consortium frequency of 63%.

§§Test only completed on 1 occasion, with subsequent efforts hampered by insufficient cells.

‖‖‖TIGER (Targeted Immuno and Gastro Enrichment) panel covering 72 genes implicated in immunodeficiency and 53 genes implicated in diseases of interest to gastroenterology.

¶¶Low for age.

##Highest of 2 repeats (range, 4301-4702 pg/mL).

***Healthy children and adults have soluble CD25 levels of less than 2500 pg/mL. Children with inflammation have levels of 2500 pg/mL or greater. To date, genetically confirmed HLHs typically have had soluble CD25 levels of greater than 5000 pg/mL, but this decreases with treatment.

†††Greatest value of 2 measurements (range, 450-472 mg/kg).

‡‡‡Greatest value of 43 measurements (7371 ng/mL).

§§§Test repeated 8 times, 2 times with normal results, 4 times absent, 1 time impaired, and 1 time unable to analyze.

TABLE E2. List of 18 candidate genes identified after homozygosity mapping and whole-exome sequencing (see main text)

Gene	Variant	Predicted effect on protein from wANNOVAR summary	Commentary
ANP32C	c.C592A: p.Q198K	Unknown	Excluded from further consideration
APC2	c.C796A:p.P266T	SIFT, T; Polyphen2, P	Excluded from further consideration
VMAC	**c.C328T:p.R110C**	**SIFT, T; Polyphen2, B**	**Variant not confirmed after Sanger sequencing (ie, false positive) and therefore discounted**
EMR1	c.A2180T:p.E727V	PolyPhen2, B; present in 1% of the population	Excluded from further consideration
KANK3	c.G2078A:p.S693N	SIFT, T; Polyphen2, D; present in 1% of the population	Excluded from further consideration
MUC16	**c.G22123C:p.A7375P**	**SIFT, D; Polyphen2, D**	**Confirmed on Sanger sequencing but ultimately deemed a biologically implausible candidate**
ZNF560	c.G1253A:p.G418D	SIFT, T; Polyphen2, B; present in 1% of the population	Excluded from further consideration
LDLR	c.G910A:p.D304N	SIFT, T; Polyphen2, B	Biologically implausible candidate; excluded from further consideration
DNASE2	**c.A284G:p.Y95C**	**SIFT, D; Polyphen2, D**	**Confirmed on Sanger sequencing; final variant selected for further in-depth functional work (see main text)**
OR10C1	c.A736T:p.M246L	SIFT – D, Polyphen2 - B	Excluded from further consideration
VARS2	**c.G2308A:p.V770M**	**SIFT, T; Polyphen2, D**	**Confirmed on Sanger sequencing; variant causes mitochondrial disease (wrong phenotype) and was ultimately excluded in patient V-2 after normal respiratory chain enzyme analysis of muscle biopsy specimen**
MUC22	c.C323G:p.T108S	No prediction	Excluded from further consideration
HLA-B	c.C341A:p.A114D c.A301G:p.S101G	SIFT, T; Polyphen2, B SIFT, T; Polyphen2, B	Biologically implausible candidate; excluded from further consideration
MICA	**c.G493A:p.V165I**	**SIFT, T; Polyphen2, B**	**Confirmed on Sanger sequencing; highly polymorphic gene, predicted nondamaging variant and therefore was excluded**
LY6G6F	**c.G442C:p.V148L**	**SIFT, D; Polyphen2, D**	**Confirmed on Sanger sequencing; involved in platelet activation and therefore a biologically less plausible candidate**
HLA-DRB5	c.C308T:p.A103V c.G307C:p.A103P	SIFT, T; Polyphen2, P SIFT, T; Polyphen2, P	Excluded from further consideration
HLA-DQA1	c.C592A:p.Q198K	SIFT, T; Polyphen2, B	Excluded from further consideration

Frequency (<0.01) in population was taken from the 1000 Genomes Project and the Exome Sequencing Project. Genes highlighted in boldface were considered for further study after filtering based on population frequency and biological plausibility (see main text).
SIFT/PolyPhen2 predictions: *D*, deleterious; *M*, medium; *P*, polymorphism; *T*, tolerated.